V European Conference on Computational Fluid Dynamics
ECCOMAS CFD 2010
J. C. F. Pereira and A. Sequeira (Eds)
Lisbon, Portugal, 14–17 June 2010

PERFORMANCE ANALYSIS OF FLOW IN A IMPELLER-DIFFUSER CENTRIFUGAL PUMPS USING CFD :SIMULATION AND EXPERIMENTAL DATA COMPARISONS

Perez J.[†], Chiva S.[†], Segala W*., Morales R.*, Negrao C.*, Julia E[†]., Hernandez L.[†]

[†]Dep. Mechanical Engineering and Construction, Jaume I University of Castellón

Campus Riu Sec, s/n, Castellón, Sapin

e-mail: schiva@emc.uji.es

[*] PPGEM/UTFPR Universidade Federal do Paraná

Av. Sete de Setembro 3165, CEP. 80230-901, Curitiba-PR-Brazil

e-mail: rmorales@utfpr.edu.br

Key words: CFD, Centrifugal Pump, Interfaces, Rotational Domains,

ABSTRACT

The design of centrifugal pumps needs a detailed understanding of the internal flow. The prediction of the flow inside the pump is comple due, mainly, to the rotation and the curved three-dimensional shape of the impellers, and its intrinsic unsteady behavior. Using computational fluid dynamics CFD codes, the flow behavior predictions are quite good in some cases, but the complex internal flows are not fully understood yet especially at off-design conditions or when internals , like diffuser, are presents. Nowadays it is very common to use CFD codes in order to investigate the behavior of that kind of flow, and the (CFD) analysis is being increasingly applied in the design of centrifugal pumps. Nevertheless, fundamental questions like the most appropriate method for modeling the rotation of the impeller and its interaction with the static diffuser remains open.

In this work the flow in a centrifugal pump, with static diffuser, has been studied using a commercial CFD code, ANSYS-CFX,[1][2] and the global performance has been compared with experimental results. The flow analysis is focus on the centrifugal pump performance and the flow characteristics under different operational conditions using CFD, and in the influence of a volute diffuser on the pressure and velocity fields inside the centrifugal pump impeller. The centrifugal pump used in the test is a commercial centrifugal pump with two stage, eight backward curved blades, and a twelve vane diffuser (model Imbil Itap 65-330/2). The experimental work has been performed at the LabPetro of the Departamento de Engenharia de Petróleo at Universidade Estadual de Campinas, Brazil.

The numerical domain calculation was divided in three sub-domains: pipe intake, first impeller and diffuser. The pipe intake domain and the diffuser was modeled in a similar way as a stationary reference frame. The first impeller geometry was modeled and the entire impeller domain rotates with a constant speed as a rotating reference frame. Different interface models were tested in the simulation.

The results obtained have been in a very good agreement with the experimental data for different pump speed. The impeller – diffuser interaction behavior is studied.

1.- INTRODUCTION

Centrifugal pumps are among the most used equipment in industrial plants. Besides that, efforts to infer the so-called pump performance curves are still required, mainly when the pump is used to transfer fluids that have a history of properties change, as the viscosity or density and chemical composition. Nowadays, it is common to use correction factor to prevent the centrifugal pump behavior when delivering different fluids. There are controversies between the uses of theses correction factors, for example, to the pump off-design conditions. Thus, computational fluid dynamics modeling may become a reasonable alternative to understand the flow behavior inside centrifugal pumps. Focusing on these aspects this work presents numerical results of the flow inside the first stage of a commercial double stage centrifugal pump delivering water. This pump is similar to a radial Electrical submersible pump, ESP, commonly used in oil wells. It was select three different impeller angular velocities: 1150rpm (nominal), 1000rpm, and 806rpm. It was used a turbulence model and the flow was considered in transient regimen. The numerical results was compared to experimental data and shown good agreement.

2.- GOVERNING EQUATIONS

To describe properly the flow behavior in centrifugal pumps the equations of conservation of mass and momentum are necessary, in the simulations the temperature is considerate isothermal without heat exchange. In this chapter a global description of the conservation equations is explained.

The model of centrifugal pump studied has been an Imbil Itap 65-330/2, the pump has a rotational piece, the rotor, and also static ones like the diffuser. The computational fluid dynamics programs allow the user to divide the model in parts called sub-domains, so every sub-domain can have different characteristics. For this case it is necessary to split the model in four different parts, three of them will be stationary and the sub-domain assigned to the rotor will have angular velocity. Thus, two different kinds of domains are coexisting in the same numerical simulation, to connect this different parts ANSYS CFX 12 provides the user the interfaces to transfer the information between different domains [3]. Every sub-domain has its own mesh.

To describe the rotational movement, first of all it is necessary to have an agreement with the reference framework of the model, this is to fix the Z vector (0,0,1) as rotational axis. And ensure that the domain assigned to the rotor shares the same rotational axis and this is passing through the (0,0,0) point of the reference framework. To describe properly the flow on this domain additional terms must be included on the momentum equations. Considering a non-inertial reference framework system (x,y,z) the equations of conservation of mass (*1.1*) and momentum (*1.2*) are described as follows:

$$\vec{\nabla} \cdot \overrightarrow{V_{xyz}} = 0 \qquad (1.1)$$

$$-\frac{1}{\rho}\nabla p + \upsilon\nabla^2\overrightarrow{V_{xyz}} + \vec{g} = 2\vec{\omega} \times \overrightarrow{V_{xyz}} + \vec{\omega} \times (\vec{\omega} \times \vec{r}) + \frac{d\overrightarrow{V_{xyz}}}{dt} + \overrightarrow{V_{xyz}} \cdot \nabla\overrightarrow{V_{xyz}} \qquad (1.2)$$

The term $2\vec{\omega} \times \overrightarrow{V_{xyz}}$ is the coriolis acceleration and $\vec{\omega} \times (\vec{\omega} \times \vec{r})$ is the centripetal acceleration. Both terms are due to the chance from a inertial reference framework system (X,Y,Z) to a non-inertial system (x,y,z). The rest of the terms present on the equations are: The pressure gradient $-(1/\rho)\nabla p$ the viscosity dissipation $\upsilon\nabla^2\overrightarrow{V_{xyz}}$ and the gravity acceleration $\vec{g}$. On the right side of the equation there are the temporal acceleration and the convective of the flow, both also can be found in the equation for static domains.

The rest of the nomenclature: ρ specific mass, p hydrostatic pressure, υ kinetic viscosity, $\overrightarrow{V_{xyz}}$ velocity of the fluid on a non-inertial reference framework system, ω angular velocity of the rotor, $\vec{r}$ position of a particle to the origin of the non-inertial reference framework system. The equation of conservation of momentum for the rest of stationary domains can be obtained from equation *(1.2)* just making the angular velocity zero $\vec{\omega} = 0$

2.1.- Turbulent Model

Numerical simulations can be classified in three groups: RANS, LES and DNS. This work can be defined as a RANS simulation, this is (Reynolds Averaged Navier-Stokes), most common on CFD's. The LES (Large Eddy Simulations) where the flux equations that are depending on time are solved for the biggest turbulences and the effect of the smaller swirling flow is modeled. There's also another kind of simulations, the DNS (Direct numerical simulations), this models solves totally the Navier-Stokes equations, it needs a high solver capability and at moment it is only applicable to microscopic scales. For the RANS simulations a basic resolution of the Navier-Stokes equations is provided and almost the whole flux is modeled,

On the present work a turbulent flow controlled by the equations of mass and momentum conservation is used, assuming the Reynolds average equations and the Boussinesq hypothesis . With this suppositions on turbulent modeling, the equations of conservation of mass *(1.3)* and momentum *(1.4), (1.5)* and *(1.6)* are described.

$$\frac{\partial\bar{u}}{\partial x} + \frac{\partial\bar{v}}{\partial y} + \frac{\partial\bar{w}}{\partial z} = 0 \qquad (1.3)$$

$$\frac{\partial \bar{u}}{\partial t}+\frac{\partial \overline{uu}}{\partial x}+\frac{\partial \overline{uv}}{\partial y}+\frac{\partial \overline{uw}}{\partial z}= \\ =-\frac{1}{\rho}\frac{\partial \bar{p}}{\partial x}+\frac{\partial}{\partial x}\left[(\upsilon+\upsilon_t)\left(2\frac{\partial \bar{u}}{\partial x}\right)\right]+\frac{\partial}{\partial y}\left[(\upsilon+\upsilon_t)\left(\frac{\partial \bar{u}}{\partial y}+\frac{\partial \bar{v}}{\partial x}\right)\right] \\ +\frac{\partial}{\partial z}\left[(\upsilon+\upsilon_t)\left(\frac{\partial \bar{u}}{\partial z}+\frac{\partial \bar{w}}{\partial x}\right)\right]+S_x \tag{1.4}$$

$$\frac{\partial \bar{v}}{\partial t}+\frac{\partial \overline{vu}}{\partial x}+\frac{\partial \overline{vv}}{\partial y}+\frac{\partial \overline{vw}}{\partial z}= \\ =-\frac{1}{\rho}\frac{\partial \bar{p}}{\partial y}+\frac{\partial}{\partial y}\left[(\upsilon+\upsilon_t)\left(2\frac{\partial \bar{v}}{\partial y}\right)\right]+\frac{\partial}{\partial x}\left[(\upsilon+\upsilon_t)\left(\frac{\partial \bar{u}}{\partial y}+\frac{\partial \bar{v}}{\partial x}\right)\right] \\ +\frac{\partial}{\partial z}\left[(\upsilon+\upsilon_t)\left(\frac{\partial \bar{v}}{\partial z}+\frac{\partial \bar{w}}{\partial y}\right)\right]+S_y \tag{1.5}$$

$$\frac{\partial \bar{w}}{\partial t}+\frac{\partial \overline{wu}}{\partial x}+\frac{\partial \overline{wv}}{\partial y}+\frac{\partial \overline{ww}}{\partial z}= \\ =-\frac{1}{\rho}\frac{\partial \bar{p}}{\partial z}+\frac{\partial}{\partial z}\left[(\upsilon+\upsilon_t)\left(2\frac{\partial \bar{w}}{\partial z}\right)\right]+\frac{\partial}{\partial x}\left[(\upsilon+\upsilon_t)\left(\frac{\partial \bar{w}}{\partial x}+\frac{\partial \bar{u}}{\partial z}\right)\right] \\ +\frac{\partial}{\partial y}\left[(\upsilon+\upsilon_t)\left(\frac{\partial \bar{w}}{\partial y}+\frac{\partial \bar{v}}{\partial z}\right)\right] \tag{1.6}$$

$$S_x=-2\omega_z\bar{v}-{\omega_z}^2x \tag{1.7}$$

$$S_y=-2\omega_z\bar{u}-{\omega_z}^2y \tag{1.8}$$

If the domain has rotation, the angular velocity must be included, in this case the source terms S_x and S_y are described in equation *(1.7)* and *(1.8)*. On static domains this source terms are zero. The turbulent kinetic viscosity υ_t is defined in equation (*1.9*)

$$\upsilon_t=\frac{\mu_t}{\rho} \tag{1.9}$$

Two equations turbulent model $\kappa-\varepsilon$ is used; this model proposes a relation between the turbulent kinetic viscosity υ_t with the turbulent kinetic energy k and the energy diffusion ratio ε, equation *(1.10)*

$$\upsilon_t=\frac{C_\mu k^2}{\varepsilon} \tag{1.10}$$

C_μ is a constant from the $\kappa - \varepsilon$ turbulent model, the equation for κ and ε are described in *(1.11)* and *(1.12)*

$$\frac{\partial k}{\partial t} + \frac{\partial uk}{\partial x} + \frac{\partial vk}{\partial y} + \frac{\partial wk}{\partial z} = D_k + P_k - k \qquad (1.11)$$

$$\frac{\partial \varepsilon}{\partial t} + \frac{\partial u\varepsilon}{\partial x} + \frac{\partial v\varepsilon}{\partial y} + \frac{\partial w\varepsilon}{\partial z} = D_k + \frac{\varepsilon}{\kappa}(C_{\varepsilon 1} P_k - C_{\varepsilon 2}\varepsilon) \qquad (1.12)$$

D_k and D_ε are the diffusive terms for κ end ε and P_k describe the production of κ, $C_{\varepsilon 1}$ and $C_{\varepsilon 2}$ are coefficients from the $\kappa - \varepsilon$ model. Description of D_k, D_ε and P_k are defined in equations *(1.13), (1.14)* and *(1.15)*

$$D_k = \frac{\partial}{\partial x}\left[\left(\upsilon + \frac{\upsilon_t}{\sigma_\kappa}\right)\frac{\partial \kappa}{\partial x}\right] + \frac{\partial}{\partial y}\left[\left(\upsilon + \frac{\upsilon_t}{\sigma_\kappa}\right)\frac{\partial \kappa}{\partial y}\right] + \frac{\partial}{\partial z}\left[\left(\upsilon + \frac{\upsilon_t}{\sigma_\kappa}\right)\frac{\partial \kappa}{\partial z}\right] \qquad (1.13)$$

$$D_\varepsilon = \frac{\partial}{\partial x}\left[\left(\upsilon + \frac{\upsilon_t}{\sigma_\varepsilon}\right)\frac{\partial \varepsilon}{\partial x}\right] + \frac{\partial}{\partial y}\left[\left(\upsilon + \frac{\upsilon_t}{\sigma_\varepsilon}\right)\frac{\partial \varepsilon}{\partial y}\right] + \frac{\partial}{\partial z}\left[\left(\upsilon + \frac{\upsilon_t}{\sigma_\varepsilon}\right)\frac{\partial \varepsilon}{\partial z}\right] \qquad (1.14)$$

$$P_k = \upsilon_t \left\{\left(\frac{\partial \bar{u}}{\partial y} + \frac{\partial \bar{v}}{\partial x}\right)^2 + \left(\frac{\partial \bar{u}}{\partial z} + \frac{\partial \bar{w}}{\partial x}\right)^2 + \left(\frac{\partial \bar{v}}{\partial z} + \frac{\partial \bar{w}}{\partial y}\right)^2 + 2\left[\left(\frac{\partial \bar{u}}{\partial x}\right)^2 + \left(\frac{\partial \bar{v}}{\partial y}\right)^2 + \left(\frac{\partial \bar{w}}{\partial z}\right)^2\right]\right\} \qquad (1.15)$$

Where σ_κ and σ_ε are the *Pradnt* number for κ and ε, the value of the coefficient of $k - \varepsilon$ are:

$$C_\mu = 0.09; \quad \sigma_k = 1.00; \quad \sigma_\varepsilon = 1.30; \quad C_{1\varepsilon} = 1.44; \quad C_{2\varepsilon} = 1.92$$

Limitations of this model will be discussed in last chapter conclusions.

3.- DOMAIN INTERFACES

In the numerical model there are 4 different domains, each of them has its own mesh. Inside the mesh the information is shared between adjacent cells. Each mesh has different characteristics, different density, number and size of cells so the problem is that two different meshes are merged and the faces of the limit cells are not matching. Some assumptions must be made in order to transfer the information across the interfaces properly.

In Ansys-CFX, two kinds of interfaces can be defined for the centrifugal pump study depending on what are they connecting. Interfaces can be connecting static meshes or connecting one static mesh with one rotational mesh.

Table 1

Type of simulation	Interface models available between stationary and rotational meshes	Interface model available between static meshes
Steady-State	*Stage / Frozen Rotor*	*GGI*
Transient State	*Stage / Frozen Rotor / Transient rotor-stator*	*GGI*

The GGI connection is the most simple of all, due to that in this case the frame is static and the relative position between cells is always the same.

If we are on a Steady-State simulation and we want to merge a static mesh with a rotational one, then we must choose between *Stage* or *Frozen rotor*. Notice that for this two interface models the relative movement between meshes is not described, internally Ansys-CFX calculate the degrees rotated by the rotor and that information is related every time step. But if we get the information of two adjacent time steps and post process the situation of the meshes we see that the relative position keeps being the same.

The last kind of interface is only available for transient simulations, this is *Transient Rotor Stator*. This last model is the only one able to report the whole relative movement between meshes it gives more accurate results but it also needs more processing time. The classification of the different interfaces is related on Table 1.

To reduce the computational time it is common to work with sections of the model, this is, split the meshes trough determinate planes and add new boundary conditions like symmetry. On the model of the pump a section model was created describing only 90º of the geometry but the development of the simulation was not the expected because in this case there's not a real symmetry plane for the flow between the blades of the pump, the behavior of the flow is very irregular and the whole geometry must be described. For the simulation of the section model new assumptions must be made and it is necessary to use the pitch change algorithm.

Between the limits of the meshes, a virtual surface with zero thickness is located. Inside This virtual surface, called control surface (C.s), the flows are conserved. This surface has to be split in different control surfaces, all the necessaries to match every control volume from both meshes from the right and for the left, see Figure 1. Every control volume has its own boundary integration points located on the limits of the interface, this points belong to one C.s (depending on the situation of them). The information of the point will be transfer to its C.s. On the other face of the C.s is the second mesh. An integration point of the second mesh will also be assigned to the C.s. The destination of information will be that integration point of the second mesh. The order is: first integration point of the mesh 1, then C.s and finally integration point on the mesh 2.

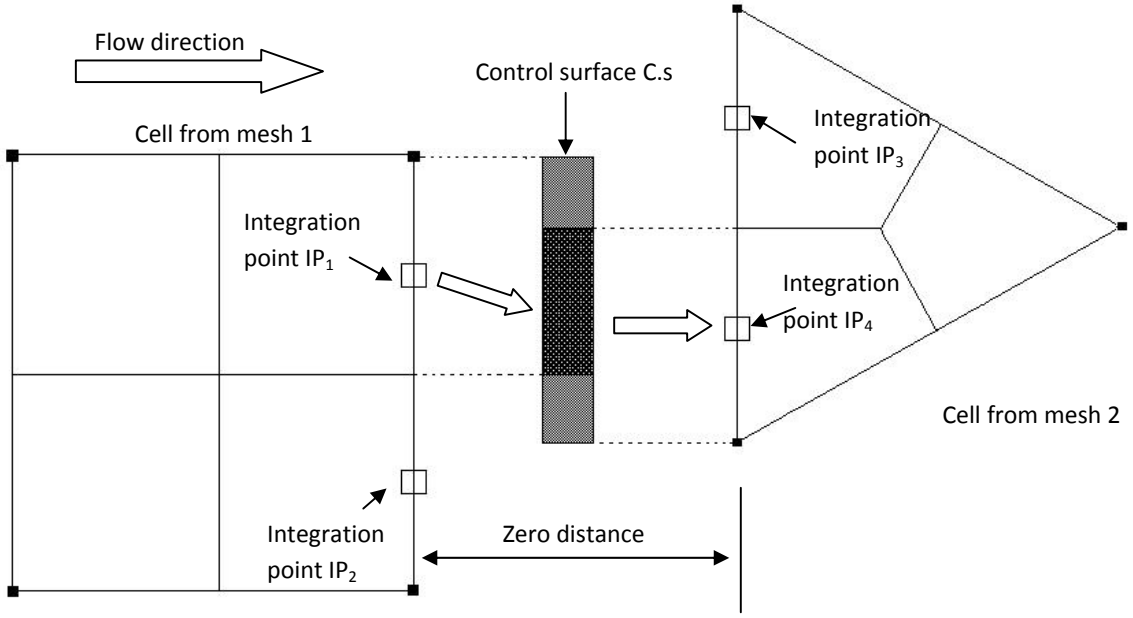

***Figure** 1: information tranfer between meshes on a GGI interface*

The C.s are split respecting into the areas assigned to the integration points (Figure 2) following Equations *(2.1),* but notice that the flux must be distributed across the different areas of the control surfaces so it must be correlated with surface fractions. Equations *(2.2)* and *(2.3)*

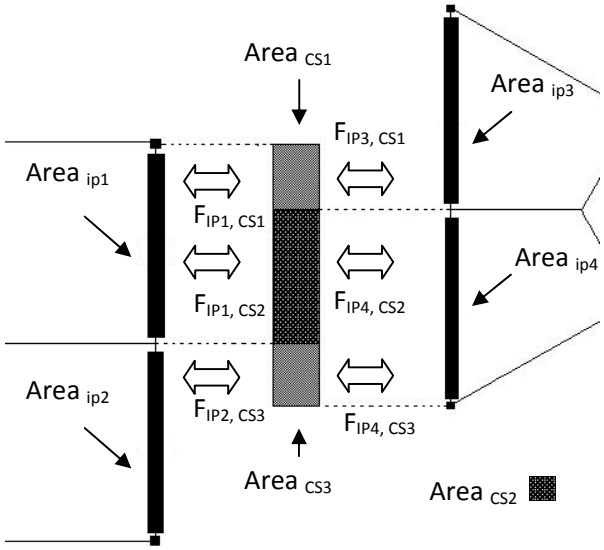

$$A_{IP1} \cap A_{IP3} = A_{SC1}$$
$$A_{IP1} \cap A_{IP4} = A_{SC2} \qquad (2.1)$$
$$A_{IP2} \cap A_{IP4} = A_{SC3}$$

$$F_{IP1,CS1} = A_{CS1} / A_{IP1}$$
$$F_{IP1,CS2} = A_{CS2} / A_{IP1} \qquad (2.2)$$
$$F_{IP2,CS3} = A_{CS3} / A_{IP2}$$

$$F_{IP3,CS1} = A_{CS1} / A_{IP3}$$
$$F_{IP4,CS2} = A_{CS2} / A_{IP4} \qquad (2.3)$$
$$F_{IP4,CS3} = A_{CS3} / A_{IP4}$$

***Figure** 2.: areas and surface fractions*

If we consider the flux that the control surface 2 (CS2) is able to see then we have: first, the flux that is coming from $Area_{IP1}$.This is from the integration point 1 (IP1) (Equation 2.4). Then this flux passes through the C.s having in count the surface fraction ($F_{IP1,CS2}$), called pitch ratio

(Equation 2.5). Now the information must go to the next mesh, this is from the surface control to the integration point IP4 (Equation 2.6), notice that here there is also a pitch ratio operation ($F_{IP4,CS2}$). And finally the flux that IP4 is able to see coming from the C. is described on Equation 2.7

$$Flux_{IP1} = \dot{m}f_{cs}\Phi_{node} \tag{2.4}$$

$$Flux_{CS} = F_{IP1,CS2} \cdot Flux_{IP1} \tag{2.5}$$

$$Flux_{CS} = F_{IP4,CS2} \cdot Flux_{IP4} \tag{2.6}$$

$$Flux_{IP4} = \dot{m}_{CS}\Phi_{CS} \tag{2.7}$$

This is the way the program has to connect the different interfaces, for the GGI connection the program only has to calculate the pitch ratio once, because both meshes are statics. When the *Transient Rotor Stator* model of interface is used, the pitch ratio for every surface control must be recalculated every time step. For the *Stage* and *Frozen Rotor* interface model the transient effects of the transport equations are not present. For the *Transient Rotor Stator* model this part of the transport equations are included, making this interface the most advisable of all. But due to the pitch ratio recalculating effort it also needs more CPU time to be solved. Sometimes the geometry of the meshes is not good enough and the meshes are not matching in some places, if this happens the interface places a wall automatically on the affected cells .

4.- IMBIL ITAP 65-330/2 DESCRIPTION

The Imbil Itap 65-330/2 is a centrifugal pump used in the oil industry, it is described as follows: the inlet of the flow is in the axial direction to the rotation axis z to the impeller, this has 8 blades and the exit of the flow is perpendicular to the z axis. The next step is the diffuser, composed by 12 blades which are orientated opposite to the rotor blades. The flow goes out of the diffuser from above to get into an inductor that drives the flow again through the z axis into the second rotor. This second stage has no diffuser and the flow is leaded through volute geometry outside the pump on perpendicular direction to the entrance. In Figures 3 and 4 the rotor and diffuser of the first stage can be observed. Only the first stage of the pump is modeled numerically (first rotor and diffuser).

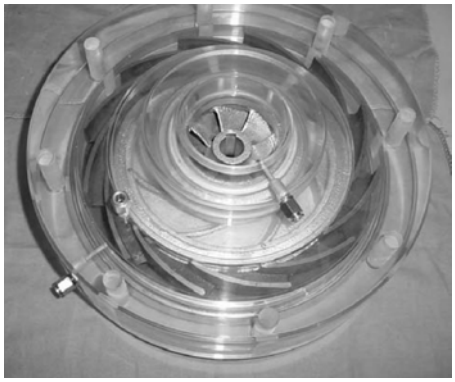

***Figure** 3: First stage of the pump Imbil Itap 65-330/2 rotor and diffuser with an acrylic tape*

***Figure** 4: difusser of the Imbil Itap 65-330/2*

5.- NUMERICAL MODEL

5.1.-Description

As was mentioned previously the numerical model (Figure 6) is divided in 4 different sub-domains, the inlet, rotor, diffuser and exit. The inlet describes a portion if pipe at the entrance of the pump, it is connected with the rotor sharing the same z axis, surrounding the rotor is the diffuser and finally below the diffuser the exit is located. The design process of the model is shown in Figure 5. The creation of the geometry was the first step. The rotor and diffuser were modeled using Ansys Workbench. Then the mesh was created with Icem, an unstructured mesh was used for the simulations (Figure 7). The whole model has around 1.5 millions cells with tetra, pyramid and penta-elements. The penta-elements are important, these volumes are the layers situated near the walls in order to describe properly the velocity gradients of the water. Information about the sub domains:

Inlet: To describe the velocities profiles at the entrance of the pump a little section of pipe is included, the length of this pipe is not enough to fully develop the flow but in order to have less cells it was decided to do it quite short. The CPU time economy in the calculations is also an important value to preserve, in further simulation a velocity profile will be provided by simulating a longer pipe.

Rotor: With 8 blades the rotor has the highest density of cells, see detail on Figure 7 the rotor has been simulated at different angular velocities: 806, 1000 and 1150 rpm.

Diffuser: Around the rotor the diffuser is located, with 12 blades the objective of this domain is to reduce the flow velocity and increase the pressure.

A recirculation phenomenon at the exit of the diffuser is given, so an extra domain has been included (the *Exit*). An opening condition is also a solution for this problem but in this way the mass flow rate cannot be imposed, the mesh of this domain is the coarsest of all.

In Table 2 the number of cells of the different domain is specified.

Table 2

Domain Name	Number of Cells
Inlet	19262
Rotor	646678
Diffuser	766654
Diffuser exit	29230
Total	1461824

Between the domains the interfaces are located. Ansys CFX provides different interfaces. If the simulations are under steady state conditions the *Stage* and *Frozen rotor* interfaces are available, if a transient simulation is chosen there is another possibility, to use a *Transient rotor-stator* model. The *Stage/Frozen-Rotor and Transient rotor-stator* models are provided to join a static part with rotational parts. To join stationary domains a GGI (general connection is used)

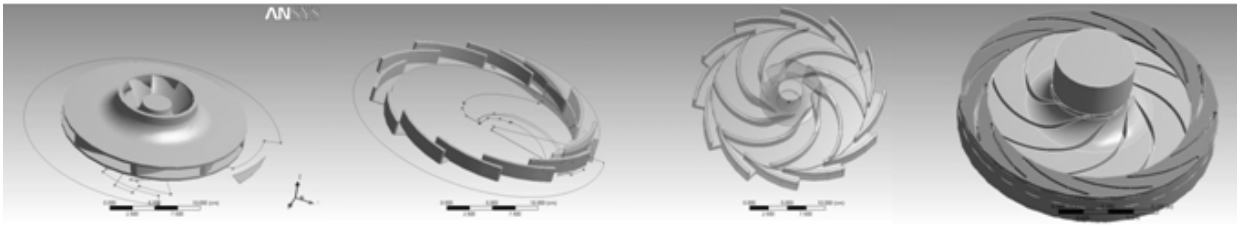

Figure 5*:Design process of the numerical model, frist the rotor , diffuers, both pieces merged and finally the totally volume of the mesh with generated pipe and exit sub-domain included.*

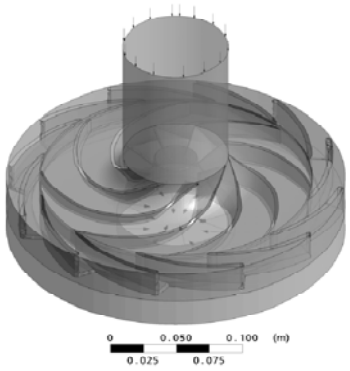

Figure 6: *Numerical model of the Imbil Itap 65-330/2*

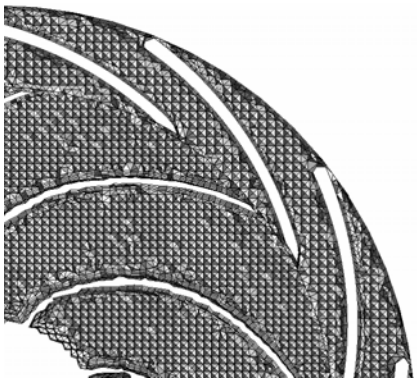

Figure 7*: Horizontal cross section on the unstructured mesh, detail of the rotor and Diffuser*

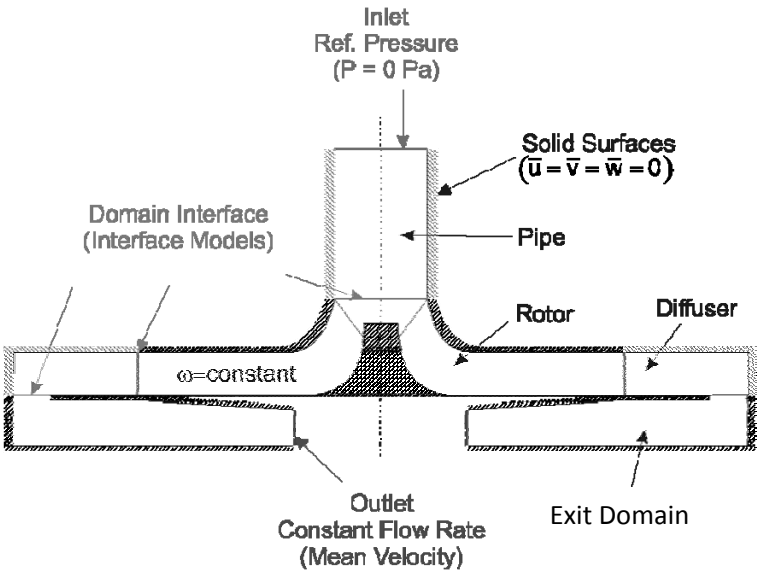

Figure 8 *:Location of the diferent sub-domains and interfaces*

Each interface is adequate depending on the type of flow. At the pump model three interfaces are located, the first one is between the inlet pipe and the rotor sub domain, the second one is connecting the rotor and the diffuser and the last one is located between the diffuser and the exit sub-domain, see details on Figure 8

The *Stage* interface is suitable when the main direction of the flow is perpendicular to the face, this is parallel to the normal vector of the cell's face. *The Frozen Rotor* interface is adequate when the direction of the flow has a relative high tangential component trough the interface surface it means perpendicular to the normal vector.

It is highly recommended to start with a steady state simulation in order to have a good converge results and then restart it in transient specifications. So for the first steady state simulations a *Stage* interface is located between the inlet and the rotor sub domain, and a *Frozen rotor* interface is located connecting the rotor and the diffuser. When the case is converged then a transient simulation can be made. The results of the present work are provided as a transient simulation so the third kind of interface can be used. The *Transient rotor stator* model is configured for the inlet-rotor and rotor-diffuser interfaces, finally a general connection GGI is located between the diffuser and the exit, both sub domains are stationary.

Notice that for a transient simulation the three kinds of interfaces are available so a comparison of the model behavior can be made for both specifications Table 3

Table 3

Transient Simulation	Interface inlet-rotor	Interface rotor-diffuser	Interface diffuser-exit
Specification 1	*Stage*	*Frozen Rotor*	*GGI*
Specification 2	*Transient rotor-stator*	*Transient rotor-stator*	*GGI*

5.2.-Simulation Conditions

In this chapter the conditions of the simulation on the numerical model of the pump Imbil Itap 65-330/2 are described. In this work a turbulent single phase flow is simulated, the fluid is water at 20°C, 997Kg/m^3 density and a dynamic viscosity of 1.00207E-3 $Pa \cdot s$. As main boundary conditions the relative pressure of 0 Pa was fixed in the inlet and the mass flow rate at the outlet of the exit domain, for the wall a non slip condition was chosen. The mass flow rate is variable from 10 to 50 m^3/h, the measure points are situated at 10-20-30-40-50 m^3/h and the angular velocity of the rotor is variable from the 806 rpm to 1150rpm. The measure points for the angular velocity are: 806-1000-1150 rpm. There are five points for each angular velocity of the rotor to perform the pressure gauge curve of the first stage of the pump.

A constant physical time step of 1E-4 is used, this generates high Courant numbers especially at 1150 rpm but it was decide not to use lower time steps to preserve the time simulation under acceptable limits. The converge criteria is reached when all the averaged residuals are under 1E-4.

The Pressure is measured as the difference between the inlet pressure and the rotor exit pressure, and also between the rotor exit pressure and the diffuser exit pressure, this provide a curve of pressure gauge for the rotor and for the diffuser, and adding both we get a curve for the pressure gauge in the first stage of the Imbil Itap 65-330/2.

The measure points on the model of the pump are shown in Figure 9, in the experiments the pressure was measured every second during a minute and then the average was calculated. The measures on the real pump were made by Segala.W and Perez Mañes.J [1,2] at the Pretolab laboratory in Unicamp University of Campinas (Sao Paulo State) Brazil in 2008. The measured points on the numerical model are analogs with the real model as it is shown in Figure 3, but in this case the value obtained is an average of all the equidistant points around the z axis.

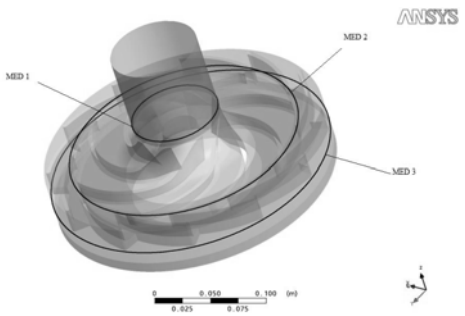

***Figure 9**: Measure lines of absolute pressure on the numerical model of the Imbil Itap 65-330/2*

6.- RESULTS AND DISCUSSION

6.1.-Pressure gauge on the different parts of the pump:

The results of the simulation show a good agreement in general terms (Figure 12), in the rotor more differences of pressure happen at high mass flow rates (Figure 10). On the diffuser (Figure 11) a lot of recirculation and swirling flow happens, this makes it more difficult to obtain a good agreement on the numerical simulation, as a result the pressure is lower than expected. Some geometry errors between the model and the real pump have been detected, mainly in the inlet configuration of the rotor, it could explain in part the pressure loss when the flow is high.

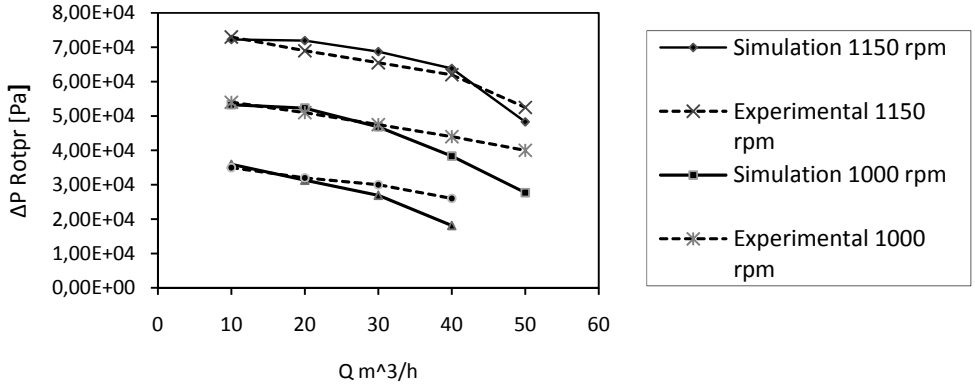

***Figure 10**: Pressure gauge of the pump Imbil Itap 65/330-2 at the rotor.*

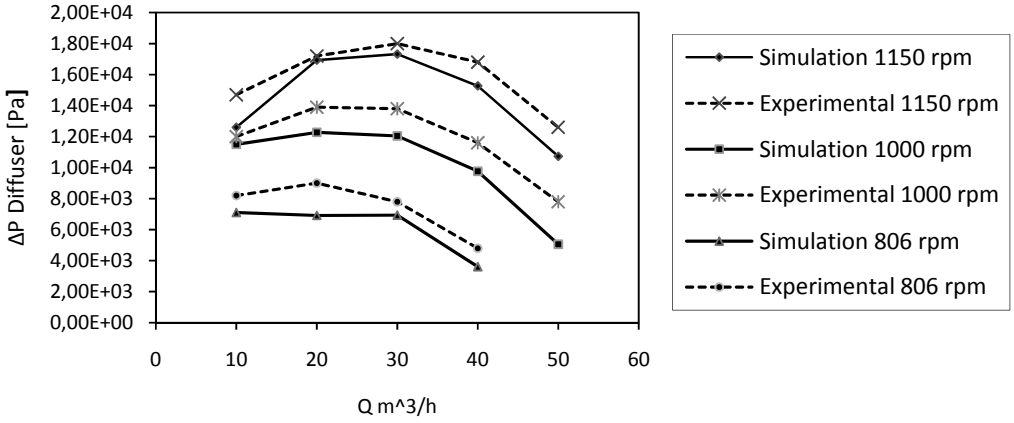

***Figure 11**: Pressure gauge of the pump Imbil Itap 65/330-2 at the diffuser.*

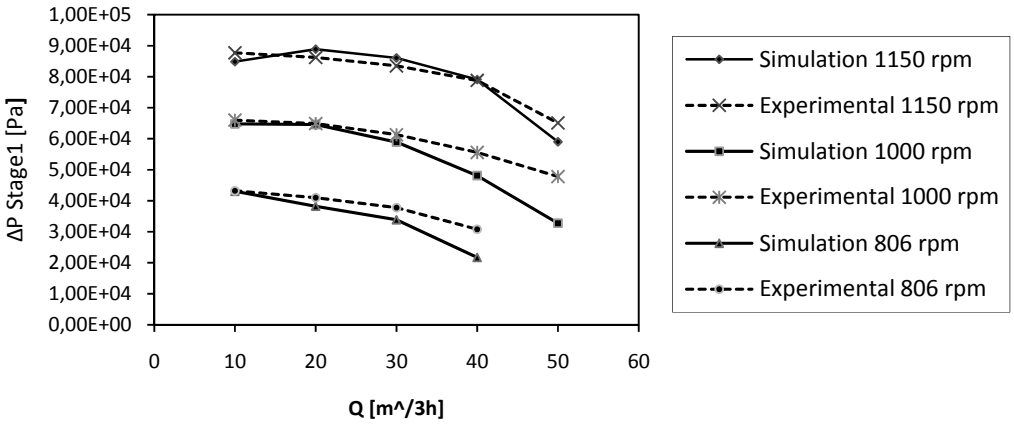

Figure 12: *Pressure Gauge of the first stage of the pump Imbil Itap 65/330-2.*

The comparison of interface models was made for a constant angular velocity of 1150 rpm. Following table 3, two different settings for the interface has been used. The result with interface *Transient Rotor Stator* has a better agreement with experimental results; with this interface the simulation is providing more pressure. Figure 13 shows the pressure differences in the rotor and the diffuser with these two configurations, as Figure 14 shows the total pressure gauge on the first stage of the pump with both configurations. This simulations have also a new improvement the previous results don't have, a fully develop velocity gradient profile as been defined in the inlet of the pipe.

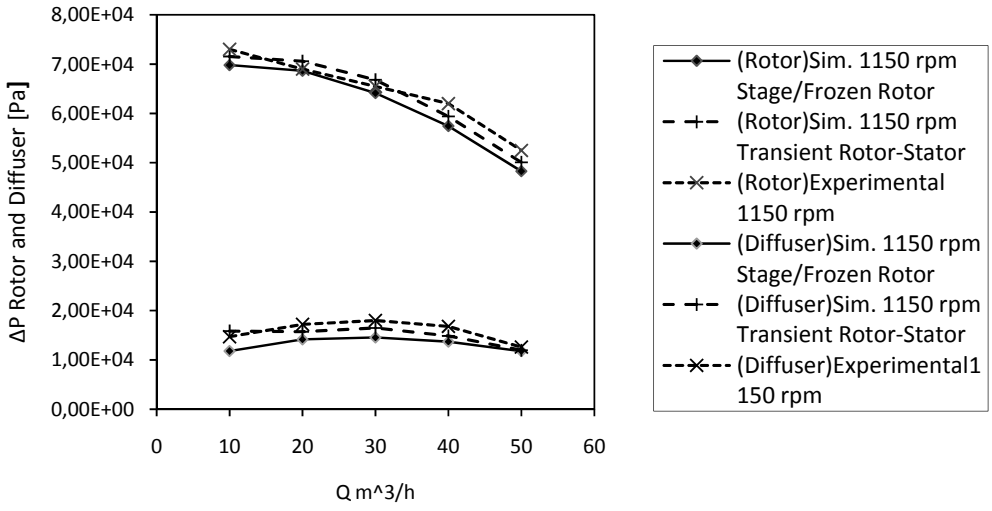

Figure 13*: Pressure gauge by Rotor and Diffuser of the pump Imbil Itap 65/330-2 using the two configurations of interfaces, Stage/Frozen Rotor and transient Rotor Stator.*

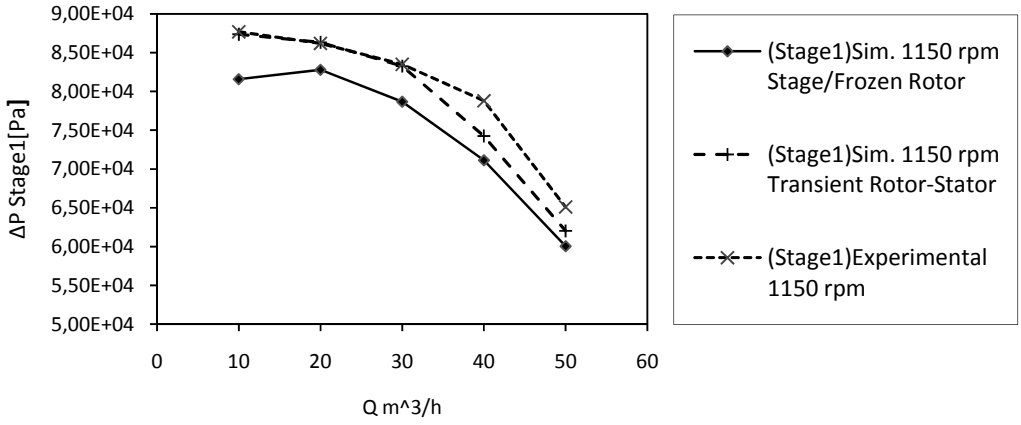

Figure 14: *Pressure gauge at the first stage of the pump Imbil Itap 65/330-2 using the two configurations of interfaces, Stage/Frozen Rotor and transient Rotor Stator.*

The curves of the pump described on Figure 10 have a characteristic loss of pressure at high mass flow rates. This effect seems to be happening also on Figure 14 but this time it is a weak effect. Thus, the development of a properly velocity gradient at the entrance of the pump seems to be important to reach the experimental pressures, especially at high mass flow rates. The differences on pressure can be regarded to the turbulent model and the influence the centrifugal field has on it. Centrifugal field cancels partially the turbulence, this is an interesting effect to study for the correct develop of the water flow. Depending on the mass flow rate different flow regimes can be observed, especially inside the diffuser. At $20m^3/h$ the behavior of the flow is very turbulent (Figure 15 and 16), and at $50m^3$ /h it is more laminar (Figure 17) .On Figures 18, 19 and 20 the pressure field at 1150 rpm can be observed for different mass flow rates.

Figure 15*: Stream lines of the flow at 1150rpm and $20m^3/h$, notice the differences between the rotor and diffuser.*

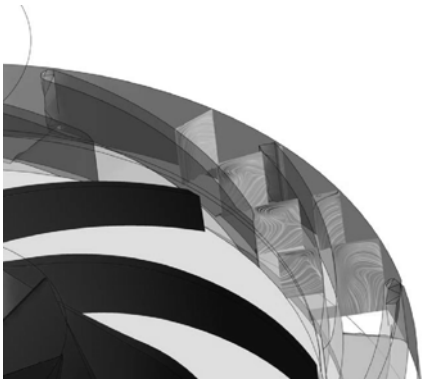

Figure 16*: Stream lines on different planes of the diffuser at 1150rpm and $20m^3/h$*

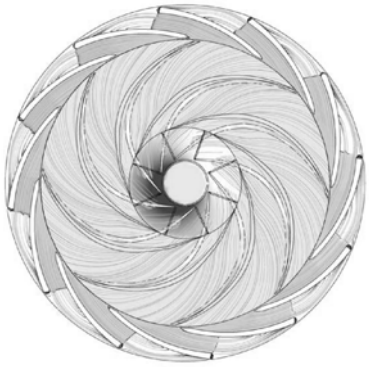

***Figure 17**: Stream lines of the flow at 50m^3/h*

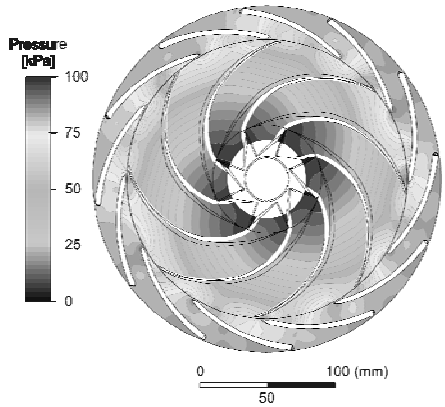

***Figure 18**: Pressure field distribution (KPa) on the pump at 1150 rpm and 20m^3/h*

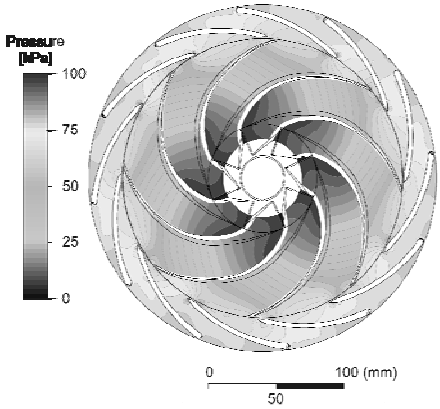

***Figure 19**: Pressure field distribution (KPa) on the pump at 1150 rpm and 35m^3/h*

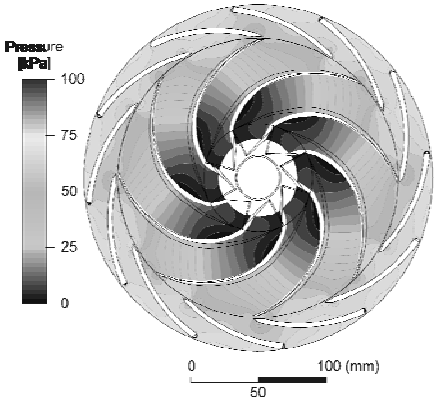

***Figure 20**: Pressure field distribution (KPa) on the pump at 1150rpm and 50m^3/h*

7.- CONCLUSIONS

In this work was simulated numerically the flow inside the first stage of a centrifugal pump composed by two stages. A single phase turbulent flow was considered in transient regime with water under constants proprieties as fluid. Four angular velocities for the rotor were simulated 1150, 1000 and 806 rpm.

From the numerical simulation curves of pressure gauge were elaborated on the rotor and diffuser depending on the mass flow rate. a good agreement was obtained compared with the experimental results obtained in the pump bench of the Unicamp University.

The pressures obtained in the numerical simulation were slightly under-predicted. The differences of pressure between experimental result and numerical results in the diffuser were bigger, an explanation for this can be found in the election if the turbulent model. It is well

known that $\kappa - \varepsilon$ turbulent model was not made for flow on curve surfaces, and it is not describing properly recirculation and swirling flow, in fact the angular velocity does not appear explicitly in the κ equation obtained by adding the normal stresses. Thus the $\kappa - \varepsilon$ model is totally blind to rotation effects. The swirling flow can be regarded as a special rotational effect with the axis usually aligned with the mean flow direction. In the rotor those phenomena are partially counter arrested for the centrifugal field but when the flow arrives at the diffuser it turns very turbulent, the diffuser has lots of recirculation and swirling flow phenomena specially at low mass flow rates, see Figures 15 and 16. Numerical results at that stage are expected to be worst and the difference in pressure is bigger. Another limitation for the $\kappa - \varepsilon$ model is that it cannot be used describing the behavior of the fluid in the near wall region when the boundary layer is detached.

With the results of the present work, further studies can be developed:

- Simulate two phase flow, as this regime flow is the most common in the industry
- Change the turbulent model to other adapted to swirling flow: SST or RST (Reynolds Stress tensor) model.
- Study the flow viscosity effect.
- Simulate the second stage of the pump.

8.- NOMENCLATURE

Symbol	Description	Units
ρ	*Density*	$kg \cdot m^{-3}$
p	*Hydrostatic pressure*	*Pa*
υ	*kinetic viscosity*	$m^2 \cdot s^{-1}$
υ_t	*turbulent kinetic viscosity*	$m^2 \cdot s^{-1}$
$\vec{g}$	*Gravity acceleration*	$m \cdot s^{-2}$
ω	*Angular velocity*	$rad \cdot s^{-1}$ *rads*
$\vec{r}$	*Vector of position of a particle from a no- inertial framework system*	*m*
$\bar{u}$	*Average velocity of Reynolds in tangential direction*	*m · s-1*
$\bar{v}$	*Average velocity of Reynolds in radial direction*	$m \cdot s^{-1}$
$\bar{w}$	*Average velocity of Reynolds in axial direction*	$m \cdot s^{-1}$
$\bar{p}$	*Pressure as Reynolds average application*	$kg \cdot m^{-1} \cdot s^{-2}$
κ	*turbulent kinetic energy*	$m^2 \cdot s^{-2}$
ε	*Turbulent energy diffusion ratio*	$m^2 \cdot s^{-3}$
t	*Variable time*	*s*
μ	*Dynamic viscosity*	$kg \cdot m^{-1} \cdot s^{-1}$
μ_t	*Turbulent viscosity*	$kg \cdot m^{-1} \cdot s^{-1}$
C_μ	*Closure law associated to turbulent viscosity*	-
D_ε	*diffusive term for transport equation of ε*	$m^2 \cdot s^{-4}$
D_κ	*diffusive term for transport equation of κ*	$m^2 \cdot s^{-3}$
P_k	*Turbulent kinetic energy production*	$m^2 \cdot s^{-3}$

$C_{\varepsilon 1}$	*Closure constant of* $\kappa - \varepsilon$ *turbulent model*	-
$C_{\varepsilon 2}$	*Closure constant of* $\kappa - \varepsilon$ *turbulent model*	-
σ_{κ}	*Prandtl number for turbulent kinetic energy* κ	-
σ_{ε}	*Prandtl number for energy dissipation* ε	-

REFERENCES

[1] Segala, W. et al. , "Centrifugal Pump Performance: Numerical Simulation and Experimental Data Comparisons". 12th Brazilian Congress of Thermal Engineering and Sciences, Belo Horizonte – Brazil, 2008.

[2] Perez, J., "*Imbil Ita 65 330/2: Ensayo Experimental y Simulación Mediante Técnicas de Mecánica de Fluidos Computacional*", MSc Thesis, Universidad Jaume I, Spain (2009)

[3] *ANSYS-CFX Sover Theory Guide*, ANSYS Inc., (2009)